A molecular simulation study of Pt stability on oxidized carbon nanoparticles

Shuai Ban, Kourosh Malek, Cheng Huang*

National Research Council of Canada, 4250 Wesbrook Mall, Vancouver, BC, Canada V6T 1W5

HIGHLIGHTS

► A molecular model of carbon nanoparticle has for the first time been developed.
► Oxidative degradation of carbon is simulated and characterized at a molecular level.
► Dynamic stability of Pt nanoparticles supported on oxidized carbon surface is studied.
► Thermal activation plays a key role in the deformation of Pt crystal structures.

ARTICLE INFO

ABSTRACT

Molecular simulation is used to model the structural change of carbon nanoparticles in terms of total mass loss during the oxidation process. The density changes as well as simulation snapshots suggest a location-dependent gasification, particularly taking place in the core of the carbon particles. A graphitic shell structure of degraded carbon particles obtained from our simulations is in agreement with experimental observations. In addition, the shrinkage of graphitic crystallites near the carbon surface leads to the formation of micropores, the volume of which increases with the oxidation level. On the basis of this carbon model, the stability of Pt nanoparticles is investigated for various temperatures and roughnesses of the carbon surface. Simulation results show that migration and coalescence of Pt particles indeed occur, but at a low rate. In particular, detachment and transport of small Pt clusters were observed from simulation snapshots, supporting the argument that the transport of molecular Pt species occurs on carbon surface. The thermal activation plays a key role in the deformation of the Pt crystal structure. During simulations, both the size and surface of Pt particles increase at elevated temperature, i.e. 600 °C. However, only a few of the surface Pt atoms may contribute to the catalytic performance due to their site-dependent reactivity.

Crown Copyright © 2012 Published by Elsevier B.V. All rights reserved.

1. Introduction

Carbon black is an important material that is commonly used as a catalyst support in proton exchange membrane fuel cell electrodes, owing to its unique electrical and structural properties. Several types of carbon blacks exist, including furnace black, channel black, lamp black, thermal black and acetylene black, the designations of which refer to the relevant manufacturing processes sharing common procedures; liquid or gaseous hydrocarbons are decomposed at elevated temperature with reduced contents of oxygen [1]. Details of pyrolysis process, carbonization of a parent feedstock, and the formation of porous carbon blacks illustrate the complexity of the reaction conditions, including rates of heating, heat treatment temperature, soak time and ambient

gases [2]. During pyrolysis (<700 °C) and carbonization (>700 °C), macromolecular networks start to form from individual carbon precursors. By increasing heat treatment temperature, the thermodynamically unstable network becomes carbonaceous and aromatic as carbon atoms readjust their positions to the six-membered ring system, forming the building blocks of the graphite-like lamellar constituent molecules [3–7]. The space elements, generally less than a few nanometers, in between these molecules constitute the microporosity of carbon black [8]. The morphology of resulting micropores depends on the structural details of lamellar constituents that are strongly affected by specific production conditions [2].

In conventional catalyst layers of fuel cells, Pt nanoparticles are highly dispersed on the carbon surface, the catalytic performance of which is controlled by the high electronic conductivity and high surface area of primary carbon black aggregates [1,9,10]. In the automotive application, the highly dynamic operation conditions bring about the issue of carbon

* Corresponding author. Tel.: +1 604 221 3050; fax: +1 604 221 3001.
 E-mail address: Cheng.Huang@nrc-cnrc.gc.ca (C. Huang).

corrosion, or oxidation, due to the excursion to high cell potentials [11]. The typical electrochemical carbon corrosion is described by $C + 2H_2O \rightarrow CO_2 + 4H^+ + 4e^-$ $E = 0.207V$ (vs. RHE) [12,13]. It is known that the spherical carbon black primary particles have an inhomogeneous graphitic structure where the concentrically graphitic order gradually diminishes towards the particle center [14]. As the oxidation resistance of graphite carbon within graphitic layers is approximately 1–2 orders of magnitude higher than that of the disordered ones in the core of carbon particles, the corrosion mainly takes place in the central region of carbon, and eventually leaves a shell-like structure dominant by graphitic carbon in the corroded carbon particles [15,16].

Since the stability of Pt catalysts supported on carbon surfaces is one of the major issues causing the loss of the fuel cell performance, it is of great importance to gain a fundamental understanding towards the structural changes of Pt nanoparticles as well as the impact of carbon corrosion on the Pt/C catalytic performance. However, to our best knowledge, few studies have been focused on molecular modeling of carbon nanoparticles and carbon related phenomena. This is mainly due to the lack of representative models of carbon nanoparticles having a diameter of 20–30 nm and containing 10^5–10^6 atoms that are often observed in TEM measurements [17]. In this study, we attempt to investigate the dynamic property of carbon supported Pt nanoparticles by using the carbon black model that we have recently developed as the initial material [18]. The structural change of carbon nanoparticles in terms of total mass loss is modeled for the oxidation process. No specific reaction mechanism for oxidant agents, e.g. O_2, H_2O, NH_3 is explicitly considered here. The examination of the complex reaction pathways from the transition state theory is, therefore, beyond the scope of this work. The structures of the oxidized carbon nanoparticles are initially validated in terms of density, carbon composition, morphology, and porosity. Thereafter, on the basis of the simplified model of oxidized carbon nanoparticles, the Pt stability on carbon external surface is investigated with emphasis on two major factors, i.e. temperature and roughness of carbon surface.

2. Simulation methods

2.1. Molecular model of carbon black primary particles

The atomic model of carbon black primary nanoparticles is adopted from our previous study [18]. Some simulation details are provided as follows. The building unit of carbon black is considered to be the hexagonal graphitic layer, the size of which mimics the level of carbon graphitization. Two typical regions of carbon particles are distinguished as amorphous core and graphitic shell. For convenience, we choose small graphitic sheets (core unit) with the diameter $d = 0.7$ nm (24 carbon atoms) to construct the amorphous core of all carbon particles. The graphitized shell is built from relatively large graphitic sheets (shell unit) with the diameters $d = 2.7$ nm (216 carbon atoms), 3.2 nm (294 carbon atoms), and 3.7 nm (384 carbon atoms), respectively. The density of the carbon particles is kept at 2 g cm^{-3}, and its porosity is expected to be negligible [1]. The carbon nanoparticle is synthesized through two steps using the non-equilibrium molecular dynamics simulation. At the first step, the amorphous core of carbon black is formed by compressing and equilibrating a certain number of core units into a spherical volume (diameter 10 nm) given the density of 2 g cm^{-3}. After that, similar compression procedure is applied to pre-inserted graphitic layers in the shell region, and generates a primary carbon particle with the diameter of 20 nm. An annealing process is performed to further equilibrate the whole carbon particle.

2.2. Simulation method of carbon oxidation

The oxidation reaction of carbon is modeled using the kinetic Monte Carlo method [19]. This method is able to trace the dynamics and time-evolution of rare-event system on the basis of reaction rates of individual events. All the reaction events are assumed to be independent, leading to a series of Poisson processes. For simplicity, a consistent reaction rate is assigned to the carbon atoms with less than three neighbors. The remaining carbon atoms within the graphitic layers are assumed to be non-reactive unless their neighboring states are changed during the oxidation process. One should notice that the exact reaction rates of carbon oxidation primarily depend on the types of oxidant agents, the characteristics of carbon samples, the mass transport of reactants, the temperature, and so forth. These complicated processes are simplified in our simulations such that no specific reaction mechanism is considered explicitly. The structural change of carbon particles is simulated in terms of carbon mass loss. The simulation of carbon oxidation is performed on an event basis, where carbon atom is selected and removed with a probability proportional to its reaction rate. Once an event is executed, the neighboring list of carbon atoms and their reaction rates are updated. The whole procedure is repeated until a certain amount of carbon atoms are removed. During the oxidation process, the structural stability of oxidized carbon particles is achieved by freezing all carbon atoms, instead of modeling the C–C bond formation. It is known that the interlayer bonding of carbon
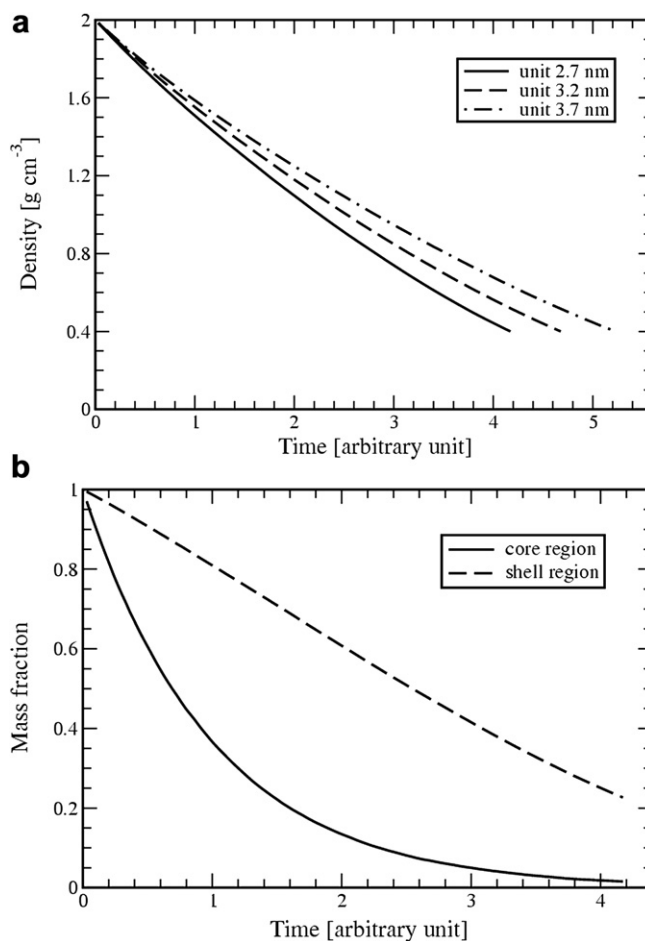

Fig. 1. Carbon weight loss during oxidation. (a) The density change of carbon black as a function of oxidation time. (b) The fraction of carbon weight loss in both core and shell regions.

fragment is responsible for the stability of carbon frameworks that often observed in experiments [16]. Employing reactive force fields that consider the bond formation, such as Tersoff's potential, is not feasible for our large carbon system, and therefore is beyond the scope of our work. The pore size distribution of the carbon particles is calculated by using the simulation code developed by Ban and Vlugt that has already shown the success in characterizing the microporosity of zeolites [20,21].

2.3. Simulation method of Pt/carbon system

To investigate the Pt stability, molecular dynamics modeling is performed using the large-scale atomic/molecular massively parallel simulator (Lammps) software [22]. EAM potential is used for Pt–Pt interaction. Lennard-Jones potential, i.e. $\sigma = 0.229$ nm and $\varepsilon = 0.085$ eV, is considered for carbon-Pt pairs, where no difference is distinguished between sp^2 carbon atoms (in the basal planes of graphene) and sp^3 carbon atoms (on the edges of graphene sheets). Carbon is kept rigid during the simulation. The reasons for neglecting carbon mobility are explained as follows. Since our current interest is in the carbon corrosion process, our model of carbon black does not consider intermolecular bonding between carbons at adjacent graphitic layers. It is known that such dangling bonds are responsible for carbon stability and can effectively prevent carbon particles from collapse. However, our non-reactive force fields of carbon may overestimate the dynamic property of carbon. In our simulations, the sizes of truncated octahedron Pt nanoparticles are chosen to be 1.5 nm (201 Pt atoms), 2.3 nm

(586 Pt atoms), and 3 nm (1289 Pt atoms). The number of each type of Pt particles is twelve, which gives a total Pt/carbon mass ratio about one. Pt nanoparticles are initially placed slightly above the surface of carbon spheres with a minimum pair distance of 1 nm. The initial configuration of Pt is equilibrated under NVT ensemble at 300 K for 500 ps, followed by a production run for 100 ns. Only Pt atoms are coupled to a Nosé–Hoover thermostat as all the carbon atoms are frozen during the simulation. The time step is set at 2 fs.

3. Results and discussion

3.1. Oxidation of carbon black

The weight loss of carbon during simulations of oxidation is shown in Fig. 1. The graphitization level of simulated carbon black is mimicked by using the graphitic layers with three different sizes, i.e. 2.7, 3.2, and 3.7 nm. All three carbon samples show the similar behavior in density change that monotonously decreases along with oxidation time. The degradation rate of carbon is in the order of 2.7 nm>3.2 nm>3.7 nm, indicating that the graphitization can slow down the oxidation process. The major reactant is the amorphous carbon with sp^3 hybridization in the core of carbon particles. The removal of sp^3 carbon will consequently affect the state of its sp^2 neighbors within the graphitic layers. In this way, the shrinkage of graphitic layers occurs. An inspection to the slope of density curves reveals that the decreasing rate of carbon density gradually slows down from 0.5 g cm^{-3} per time unit to around 0.25 g cm^{-3} per time unit. The reason for this is that the carbon particle initially
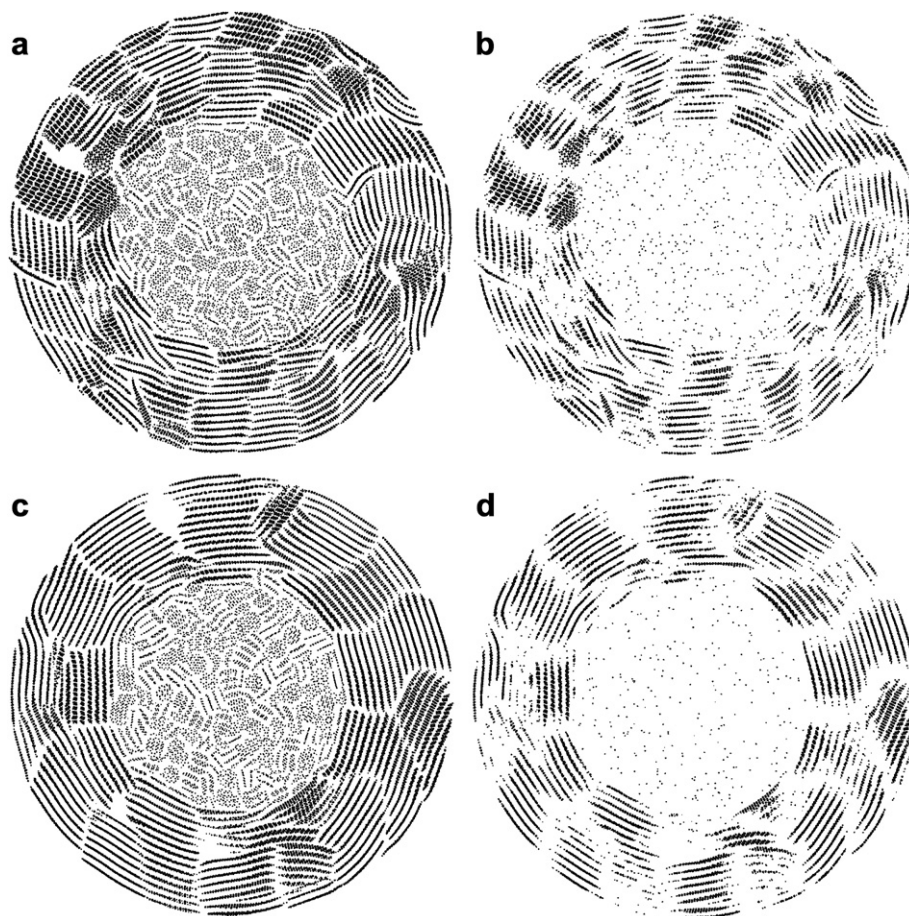

Fig. 2. Simulation snapshots of carbon black particles during oxidation. (a) The pristine carbon black particle with 2.7 nm graphitic layers. (b) The oxidized carbon black with 50% weight loss. (c) The pristine carbon black particle with 3.7 nm graphitic layers. (d) The oxidized carbon particle with 50% weight loss.

has a large amount of amorphous carbon located in the core region of carbon particles. Once the oxidation takes place, these carbon species will be primarily gasified, and leave carbon particles with a highly graphitic shell [15,16]. Such a site-dependent oxidation reaction is represented in Fig. 1b. By tracing the loss of carbon atoms at two different regions, a fast decay is observed for carbon in the core while an approximately linear decline is for carbon in the shell.

The changes of carbon structures during the oxidation are visualized in Fig. 2. For the initial carbon black, a clear separation of core and shell regions is observed. The orientation of carbon units in the core shows a random trend, while a concentric arrangement is found for the graphitic layers in the shell. In our simulations, the carbon sphere contains a core domain with the diameter of about 10 nm covered by a 5 nm thick graphite shell. One needs to note that the realistic carbon particles may have a different portion of graphitic carbon from our representative models, and the interface between core and shell region normally possesses a gradual transformation instead of a clear boundary. As a comparison, a carbon particle with 50% weight loss is shown in Fig. 2b. Two major changes are noticed. (1) Amorphous carbon in the core region is heavily oxidized, contributing a large portion to the total weight loss of the carbon particle. (2) The graphitic layers in the shell region shrink due to the slow oxidation process occurring from disordered carbon on the graphite edges. Micropores are created between adjacent graphitic crystallines. The similar tendency has also been observed between carbon black consisting of graphitic layers with the size of 2.7 nm and 3.7 nm. The only difference is that the carbon particle with larger graphitic layers has a carbon shell with a higher graphitic content than the previous one, and the removal of amorphous carbon in the core is more complete.

In Fig. 3, the pore size distribution of oxidized carbon is plotted as a function of weight loss. The pristine carbon black has a pore volume of 0.016 ml g^{-1}, indicating a nonporous structure. As shown in Fig. 3a, upon oxidation, the pore volume exhibits a quadratic growth and the mean pore diameter evenly increases. The similar trend has also been observed experimentally by Lefèvre et al. for Fe-based electrocatalysts [23,24]. During the heat treatment of carbon black in NH_3 atmosphere where the oxidation reaction occurs as $C + NH_3 \rightarrow HCN + H_2$, the total surface area as well as the volume of meso- and macropores (>50 nm) gradually increase. However, the micropore volume rises to a maximum followed by a decrease when further heated. The evolution of carbon porosity during oxidation can be understood as follows. The loss of carbon atoms results in a universal growth of carbon porosity, either internally (within carbon primary particles) or externally (between carbon particles). The external pore is contributed by the increase of macropores as well as a portion of mesopores, while the internal pore is mainly related to micropores. The general definition of micropores is the pores smaller than 2 nm. Once the size of internal micropores exceeds this threshold, they transform into mesopores, leading to the decrease of micropore volume after intensive oxidation. However, such a transition does not occur in our simulation, where the pore diameter does not reach the mesoporous region even after extensive weight loss of carbon. This mismatch is attributed to the fact that dynamics of carbon atoms is not considered in our simulations. Phenomena such as local collapse of carbon framework, aggregation of carbon fragment, etc. will enhance the formation of pores. To verify the impact of graphitization level, the pore size distributions are calculated for carbon particles with different sizes of graphitic layers in Fig. 3b. It was found that larger graphitic layers lead to a higher magnitude of large pores (>0.5 nm) but a smaller amount of tiny pores (<0.5 nm) than smaller layers. This is due to the strong resistance of graphite
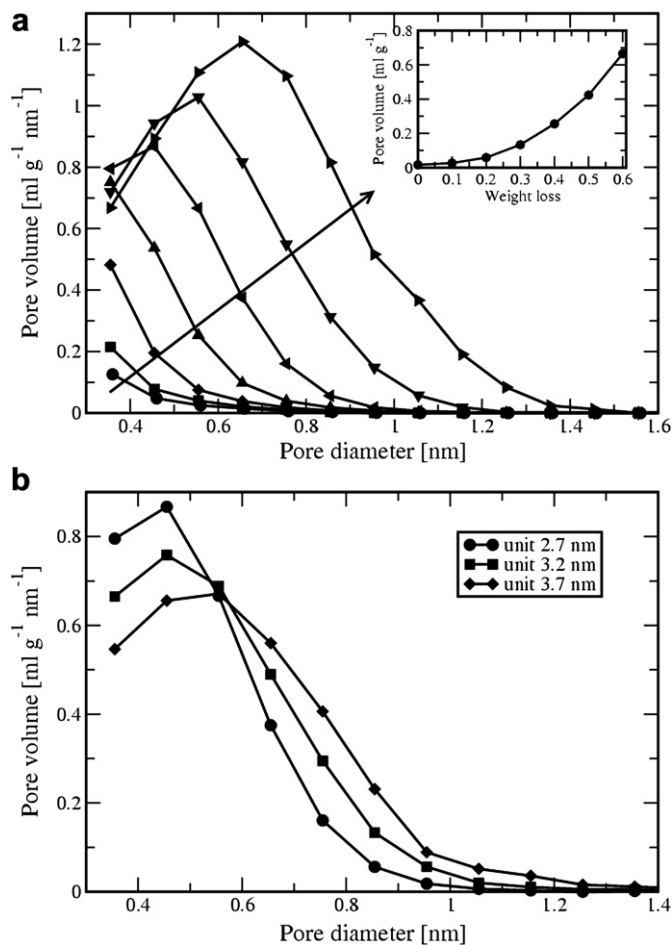

Fig. 3. The pore size distribution of carbon black particles during oxidation. (a) The pore size distributions and pore volumes of oxidized carbon black with 2.7 nm graphitic layers with 10−60% weight loss. (b) The pore size distributions of oxidized carbon black with different graphitic layers with 40% weight loss.

to oxidation reactions. For highly graphitized carbon, the amorphous carbon will be gasified more completely in the core region while the damages in the graphitic shell are relatively small.

In summary, the structural properties of oxidized carbon nanoparticles are generally validated with respect to bulk density, carbon composition, morphology, and porosity. Although a simplified approach is employed to model carbon oxidation process, the essential characteristic of oxidized carbon particles is well reproduced in our simulations. The resulting carbon structure, especially the external surface of carbon particles, will be used to study the dynamic property of Pt nanoparticles.

3.2. Pt nanoparticles on carbon surface

The stability of Pt nanoparticles is investigated in relation to two factors: temperature and surface roughness of oxidized carbon. Simulation snapshots of Pt particles equilibrated on carbon surface at 300 K and 873 K are shown in Fig. 4. A direct inspection reveals that (1) a high temperature results in a less defined crystal structure of Pt particles and (2) the roughness of oxidized carbon surface does not have a visible effect on the Pt structure. At 300 K, Pt particles possess well-defined structures of truncated octahedron, where the [111] and [100] facets are distinguishable. This structural property still exists, but in a weak manner, at 873 K in Fig. 4b. It is important to notice that coalescence of neighboring Pt particles do
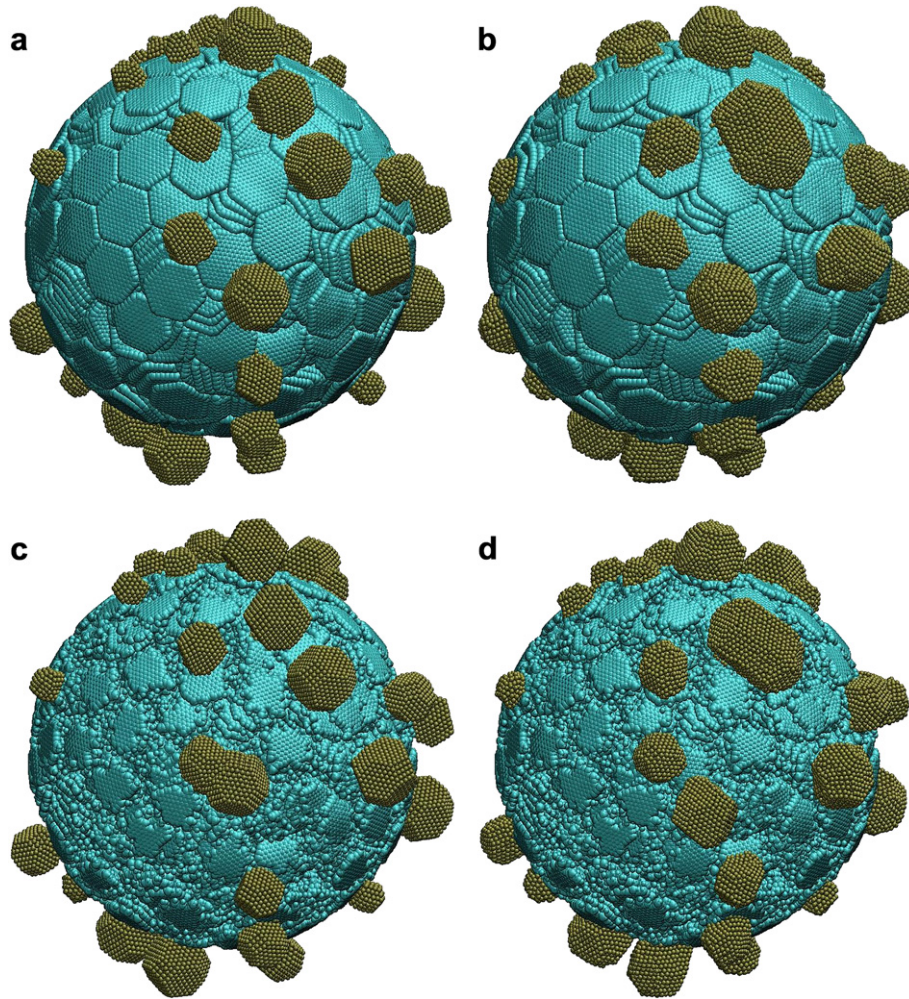
Fig. 4. Simulation snapshots of Pt particles equilibrated on the surface of carbon black with 3.2 nm graphitic layers. (a) Pt particles on the surface of pristine carbon at 300 K. (b) Pt particles on the surface of pristine carbon at 873 K. (c) Pt particles on the surface of oxidized carbon black with 50% weight loss at 300 K. (d) Pt particles on the surface of oxidized carbon black with 50% weight loss at 873 K.

take place at elevated temperatures. Similar in-situ observation by TEM has been reported by Antolini [25]. The slow surface diffusion coefficient ($\sim 10^{-20}$ cm^2 s^{-1}) derived from their work is generally in line with our simulation results that Pt particles only travel in a short range even after an long equilibration time of 100 ns.

In addition, a quantitative analysis of the size distributions of Pt particles is shown in Table 1. The size of the Pt particle is represented by the number of Pt atoms. The thermal impact on Pt structure is presented by two means, namely coalescence and

abruption. The coalescence is reflected from the appearance of large Pt particles containing more than 1289 Pt atoms (the largest Pt particle in initial configuration). Small Pt particles with a relatively high mobility can attach to the neighboring Pt particles, resulting in a necking structure. The abruption is indicated by the emergence of small Pt particles consisting of less than 201 Pt atoms (the smallest Pt particle in initial configuration). The roughness of carbon surface facilitates the Pt abruption at elevated temperature. In particular, small clusters containing only a few Pt atoms appear

Table 1
The size distribution of Pt particles on the surface of carbon black with 3.2 nm graphitic layers. The neighboring distance of Pt pairs is taken as 0.3 nm.

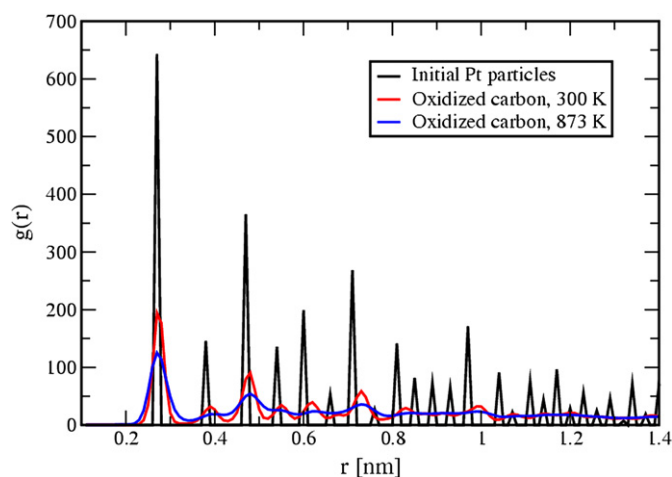| Original carbon, 300 K		Original carbon, 873 K		Oxidized carbon, 300 K		Oxidized carbon, 873 K	
$N_{particle}$	N_{atom}	$N_{particle}$	N_{atom}	$N_{particle}$	N_{atom}	$N_{particle}$	N_{atom}
12	201	3	2	11	201	1	2
12	586	9	201	11	586	1	4
12	1289	1	584	10	1289	1	195
		9	586	1	1490	9	201
		1	988	1	1875	12	586
		1	1287			8	1289
		7	1289			2	1490
		1	1488			1	2578
		1	1875				
		1	2578				

Fig. 5. The radial distribution function of the Pt particles on oxidized carbon black with 3.2 nm graphitic layers with 50% weight loss.

on oxidized carbon surface at 873 K. Due to the effect of thermal activation and the presence of carbon surface grains, small Pt clusters can detach from primary Pt particle and move in the gaps between degraded graphitic crystallites. To our surprise, this finding is consistent to the early proposed Pt degradation process by Bett et al. [26], who addressed that Pt transport would occur via transport of molecular Pt species on carbon supports.

The structure of the Pt particles was examined in terms of the radial distribution function in Fig. 5. The initial Pt in the truncated octahedral shape shows sharp peaks with a minimum pair distance of 0.27 nm. At elevated temperature, those peaks are gradually smoothed out, indicating a degeneration of Pt crystallinity. Such a degradation of Pt particles may have a negative impact on its catalytic performance due to the loss of electrochemically active surface area. To address this issue, the Pt surface area is calculated by means of Pt coordination in Fig. 6. The thermal fluctuation results in a significant difference of the Pt coordinate numbers between 300 K and 873 K. Starting from a truncated octahedral structure, about half of the Pt atoms are located inside the Pt particles (coordinate number 12) and the remaining on the surface (coordinate number 6, 7, 8, 9). The equilibration simulation broadens the distribution of Pt coordination. By assuming surface Pt atoms have a coordinate number less than ten, the fraction of

surface Pt atoms at 300 K is 0.43 while this value increases to 0.58 at 873 K. More atoms are exposed on the surface of Pt particles at the high temperature. However, it is speculated that only a few of them may contribute to the electrochemical activity as the chemical adsorption energy of surface Pt atoms is site-dependent [27]. One should notice that these conclusions are primarily for understanding the microstructure evolution during carbon corrosion process. Chemical reactions during Pt degradation, Pt dissolution, and Pt oxide formation are not explicitly considered in our simulations.

4. Conclusions

The carbon oxidation process has been simulated by using the model of carbon black nanoparticles that was developed in our previous work. The primary carbon particle features a core-shell structure, where graphitic layers arrange concentrically near the surface of carbon. This tendency diminishes towards the center, leading to a core primarily containing amorphous carbon. On the basis of weight losses and molecular snapshots of oxidized carbon, simulation results show that the gasification is mostly taken place inside the carbon core, where a shell structure of graphite is formed. This is attributed to the strong resistance of graphitic carbon to chemical degradation. As expected, the internal porosity of carbon increases with carbon oxidation level. Micropores are formed gradually between graphitic crystallites as a result of graphitic layers shrinkage during oxidation.

On the basis of the oxidized carbon model, the stability of Pt particles is investigated with respect to two major factors; temperature and roughness of carbon surface. The coalescence of Pt is observed from simulation snapshots, especially at elevated temperature. The small Pt particles with relatively high mobility can migrate and merge into neighboring Pt particles to form a necking structure. However, from a dynamic view, our simulations indicate a very slow surface diffusion of Pt particles, and consequently a low probability of Pt coalescence, particularly at ambient conditions. The transport of small Pt clusters is particularly evident from our simulations. The gaps between the oxidized graphitic layers facilitate the detachment and movement of small Pt clusters. Apart from the carbon surface roughness, the thermal activation plays a key role in the deformation of Pt crystallinity. Although more Pt atoms are exposed on the surface of the Pt particles at elevated temperature, it is speculated that only a few of them may actually contribute to the electrochemical activity of Pt/C catalysts because of their site-dependent reactivity.

References

[1] M. Wissler, J. Power Sources 156 (2006) 142–150.
[2] L. Rothbuhr, J. Witte, US patent 4292291.
[3] R.D. Heidenreich, W.M. Hess, L.L. Ban, J. Appl. Crystallogr. 1 (1968) 1–19.
[4] J.B. Donnet, R.C. Bansal, M.J. Wang, Carbon Black: Science and Technology, Marcel Dekker INC., New York, 1993.
[5] J.B. Donnet, E. Custodero, Carbon 30 (1992) 813–815.
[6] A.E. Austin, W.A. Hedden, Ind. Eng. Chem. 46 (1954) 1520–1524.
[7] L.E. Alexander, E.C. Sommer, J. Phys. Chem. 60 (1956) 1646–1649.
[8] F. Stoeckli, A. Guillot, A.M. Slasli, D. Hugi-Cleary, Carbon 40 (2002) 211–215.
[9] A. Guha, W. Lu, J. Zawodzinski, D.A. Schiraldi, Carbon 45 (2007) 1506–1517.
[10] J. Zhang, PEM Fuel Cell Electrocatalysts and Catalyst Layers: Fundamentals and Applications, Springer, 2008.
[11] C.W.B. Bezerra, L. Zhang, H. Liu, K. Lee, A.L.B. Marques, E.P. Marques, H. Wang, J. Zhang, J. Power Sources 173 (2007) 891–908.
[12] X. Yu, S. Ye, J. Power Sources 172 (2007) 145–154.
[13] F. Xu, M. Wang, Q. Liu, H. Sun, S. Simonson, N. Ogbeifun, E. Stach, J. Xie, ECS Trans. 33 (2010) 1281–1294.
[14] J.B. Donnet, Carbon 32 (1994) 1305–1310.
[15] K. Kamegawa, K. Nishikubo, H. Yoshida, Carbon 36 (1998) 433–441.
[16] G.A. Gruver, J. Electrochem. Soc. 125 (1978) 1719–1720.
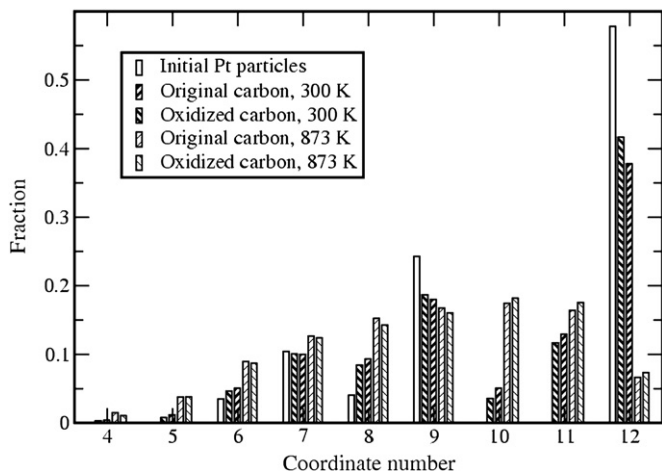[17] W. Zhu, D.E. Miser, W. Geoffrey Chan, M.R. Hajaligol, Carbon 42 (2004) 1841–1845.

Fig. 6. The coordination of Pt atoms on the surface of carbon black with 3.2 nm graphitic layers.

[18] S. Ban, K. Malek, C. Huang, Z. Liu, Carbon 49 (2011) 3362–3370.
[19] W.M. Young, E.W. Elcock, Proc. Phys. Soc. 89 (1966) 735–746.
[20] S. Ban, T.J.H. Vlugt, Mol. Simulat. 35 (2009) 1105–1115.
[21] L.D. Gelb, K.E. Gubbins, Langmuir 15 (1998) 305–308.
[22] S. Plimpton, J. Comput. Phys. 117 (1995) 1–19.

[23] M. Lefèvre, E. Proietti, F. Jaouen, J.P. Dodelet, ECS Trans. 25 (2009) 105–115.
[24] M. Lefèvre, E. Proietti, F. Jaouen, J.P. Dodelet, Science 324 (2009) 71–74.
[25] E. Antolini, J. Mater. Sci. 38 (2003) 2995–3005.
[26] J.A.S. Bett, K. Kinoshita, P. Stonehart, J. Catal. 41 (1976) 124–133.
[27] L. Wang, A. Roudgar, M. Eikerling, J. Phys. Chem. C 113 (2009) 17989–17996.